CHEMISTRY OF MATERIALS
Article

Chem. Mater. **2010,** *22,* 5065–5073 5065
DOI:10.1021/cm1017163

Synthesis, Characterization, and Thermal Stability of $Li[Ni_{1/3}Mn_{1/3}Co_{1/3-z}(MnMg)_{z/2}]O_2$

Wenbin Luo,[†,‡] Xinhai Li,[‡] and J.R. Dahn*[,†]

[†]*Department of Physics and Atmospheric Science, Dalhousie University, Halifax B3H3J5, Canada, and* [‡]*School of Metallurgical Science and Engineering, Central South University, Changsha 410083, P. R. China*

Received June 19, 2010

$LiNi_{1/3}Mn_{1/3}Co_{1/3-z}(MnMg)_{z/2}O_2$ ($0 \le z \le 1/3$) samples were prepared from hydroxide precursors. The hydroxide precursors were heated with Li_2CO_3 at 900 °C for 3 h to prepare the oxides. The XRD results show single phase $LiNi_{1/3}Mn_{1/3}Co_{1/3-z}(MnMg)_{z/2}O_2$ samples can be prepared for $0 \le z \le 1/3$. Rietveld refinements of XRD data show that when Mn and Mg substitute for Co in NMC there is an increase in the amount of transition metal in the Li layer. Electrochemical studies of the $LiNi_{1/3}Mn_{1/3}Co_{1/3-z}(MnMg)_{z/2}O_2$ ($0 \le z \le 1/3$) samples were used to measure the rate of capacity reduction with z, found to be about −250 (mAh/g)/($z = 1$) charging to 4.3 V and −150 (mA h/g)/($z = 1$) charging to 4.6 V. The impact of Mn and Mg cosubstitution on the thermal stability of charged $LiNi_{1/3}Mn_{1/3}Co_{1/3-z}(MnMg)_{z/2}O_2$ ($0 \le z \le 1/3$) samples in electrolyte was studied using accelerating rate calorimetry. The thermal stability of $LiNi_{1/3}Mn_{1/3}Co_{1/3-z}(MnMg)_{z/2}O_2$ is independent of z for the samples studied.

Introduction

Lithium intercalation in Li_xCoO_2 was first discovered by Goodenough's group in 1980.[1] Rechargeable carbon/$LiCoO_2$ batteries were commercialized by Sony in 1991.[2] $LiCoO_2$ has dominated the Li-ion battery positive electrode material market due to its high energy density, ease of synthesis and cycling stability. However, the high cost of cobalt and safety issues associated with Li_xCoO_2 charged to high potentials has driven worldwide efforts to explore alternative materials.

Dahn's and Ohzuku's groups first reported the structure and electrochemical performance of the mixed metal oxides $Li[Ni_xMn_xCo_{1-2x}]O_2$ with either $x \approx 1/3$ or $x = 1/3$.[3,4] Much research has been performed to study the reaction mechanisms and optimize these and similar materials by new synthesis methods, applying coatings and including substituents for Ni, Mn, and/or Co.[5−12]

The impact of Al substitutions on the thermal stability of charged layered lithium transition metal oxides in nonaqueous electrolytes is well-known. The thermal stability of Al-substituted $Li[Co_{1-z}Al_z]O_2$,[13−15] $Li[Ni_{1-z}Al_z]O_2$,[16] $Li[Ni_{1/3}Mn_{1/3}Co_{1/3-z}Al_z]O_2$,[17] and $Li[Ni_{0.4}Mn_{0.4}Co_{0.2-z}Al_z]O_2$[18] increases as the Al content increases.

Luo and Dahn carefully studied the crystal chemistry and electrochemical properties of Mg-substituted $LiCoO_2$.[19] There have been reports that Mg substitution for Ni, Mn or Co in $Li[Ni_{(1/3-z)}Mn_{(1/3-z)}Co_{(1/3-z)}Mg_z]O_2$ and Mg substitution for Ni in $Li[Ni_{(0.6-x)}Mg_xCo_{0.25}Mn_{0.15}]O_2$[20,21] all improve the thermal stability of the charged electrode materials. The Dahn group studied the effect of Al and Mg substitutions in $LiNi_{1/3}Mn_{1/3}Co_{1/3}O_2$. The results showed that, unlike the case of Al substitution for Co in NMC, Mg

*Corresponding author. E-mail: jeff.dahn@dal.ca.

(1) Mizushima, K.; Jones, P. C.; Wiseman, P. J.; Goodenough, J. B. *Mater. Res. Bull.* **1980**, *15*, 783.
(2) Nagaura, T. *Prog. Batteries Battery Mater.* **1991**, *10*, 218.
(3) Lu, Z.; MacNeil, D. D.; Dahn, J. R. *Electrochem. Solid-State Lett.* **2001**, *4*, A200.
(4) Ohzuku, T.; Makimura, Y. *Chem. Lett.* **2001**, 642.
(5) Xiao, J.; Chernova, N. A.; Whittingham, M. S. *Chem. Mater.* **2008**, *20*, 7454.
(6) Chen, Z.; Sun, Y. K.; Amine, K. *J. Electrochem. Soc.* **2006**, *153*, A1818.
(7) Wilcox, J.; Patoux, S.; Doeff, M. *J. Electrochem. Soc.* **2009**, *156*, A192.
(8) Shaju, K. M.; Bruce, P. G. *Adv. Mater.* **2006**, *18*, 2330.
(9) Hwang, B. J.; Tsai, Y. W.; Carlier, D.; Ceder, G. *Chem. Mater.* **2003**, *15*, 3676.
(10) Yin, S. C.; Rho, Y. H.; Swainson, I.; Nazar, L. F. *Chem. Mater.* **2006**, *18*, 1901.
(11) Park, S. H.; Shin, H. S.; Myung, S. T.; Yoon, C. S.; Amine, K.; Sun, Y. K. *Chem. Mater.* **2005**, *17*, 6.
(12) Zeng, D.; Cabana, J.; Bréger, J.; Yoon, W. S.; Grey, C. P. *Chem. Mater.* **2009**, *21*, 2733.
(13) Luo, W.; Dahn, J. R. *Abstracts of the 214th Meeting of the Electrochemical Society*; Honolulu, HI, Oct 12−17, 2008; The Electrochemical Society: Pennington, NJ, 2008; abstract 599.
(14) Luo, W.; Dahn, J. R. *Chem. Mater.* **2009**, *21*, 56.
(15) Luo, W.; Dahn, J. R. *Electrochim. Acta* **2009**, *54*, 4655.
(16) Ohzuku, T.; Ueda, A.; Kouguchi, M. *J. Electrochem. Soc.* **1995**, *142*, 4033.
(17) Luo, W.; Zhou, F.; Zhao, X.; Lu, Z.; Li, X.; Dahn, J. R. *Chem. Mater.* **2010**, *22*, 1164.
(18) Croguennec, L.; Bains, J.; Ménétrier, M.; Delmas, C. *Abstracts of the 216th Meeting of the Electrochemical Society*; Vienna, Austria, Oct 4−9, 2009; The Electrochemical Society: Pennington, NJ, 2009; abstract 406 .
(19) Luo, W.; Dahn., J. R. *J. Electrochem. Soc.* **2010**, *157*, A782.
(20) Kim, G.; Myung, S.; Kim, H.; Sun, Y. *Electrochim. Acta* **2006**, *51*, 2447.
(21) Liao, P.; Duh, J.; Sheu, H. *J. Power Sources.* **2008**, *183*, 766.

Published on Web 08/03/2010

substitution for Ni, Mn, or Co in NMC yields no significant improvement in thermal stability.[17]

Oh et al. reported that the charge−discharge capacity retention of zirconium-doped $LiNi_{0.8}Co_{0.2}O_2$ cathode materials was superior to the pristine cathode, especially when they were tested to a high voltage cutoff.[22] According to Y−K. Sun et al., Zr doped $Li[Ni_{0.45}Co_{0.1}Mn_{0.45-x}Zr_x]O_2$ ($x = 0.02$) shows better cycling performance and stable thermal stability. According to DSC results, the major exothermic reaction between the charged electrode material and electrolyte was delayed from 252 to 289 °C.[23] K−H. Jeong et al. found that a Zr-doped $LiNi_{0.5}Mn_{0.5}O_2$ electrode shows about 50 mA h/g higher capacity than that of the pristine $LiNi_{0.5}Mn_{0.5}O_2$ electrode and has a better thermal stability.[24] The Dahn group studied the effect of Zr substitutions $LiNi_{1/3}Mn_{1/3}Co_{1/3}O_2$. The results showed that the impact of Zr-substitutions, from a safety standpoint, is minimal.[25]

It is important to study the impact of other substituents, such as equal amounts, $z/2$, of Mn^{4+} and Mg^{2+} for z Co^{3+}, on the capacity and thermal stability of layered lithium transition metal oxides in a careful and systematic manner as was done in references.[17] In this paper, Mn and Mg cosubstituted NMC samples were prepared. The synthesis, structure and electrochemical properties of $Li[Ni_{1/3}Mn_{1/3}Co_{1/3-z}(MnMg)_{z/2}]O_2$ ($0 \le z \le 1/3$) were characterized carefully. In addition, the reactivity of the charged electrode materials with electrolyte was measured using accelerating rate calorimetry.

2. Experimental Section

2.1. Material Preparation. A $LiOH \cdot H_2O$ (Sigma Aldrich, 98%+) solution and a mixed solution of $Ni(NO_3)_2 \cdot 6H_2O$(Sigma Aldrich, 97%+), $Mn(NO_3)_2 \cdot 4H_2O$(Sigma Aldrich, 97%+), $Co(NO_3)_2 \cdot 6H_2O$(Sigma Aldrich, 98%+), and $Mg(NO_3)_2 \cdot 6H_2O$ (Sigma Aldrich, 98%+) were simultaneously added over the course of about 30 min to a stirred flask using a two-channel peristaltic pump (Masterflex C/L pump, Barnant Co.). The concentrations of the solutions were adjusted to set the (Mn+Mg):(Ni+Mn+Co+Mg) ratio. The precipitate was separated by centrifuging (Centra GP8R, International Equipment Company) and was washed with distilled water several times to remove any dissolved salts, and was then dried at 80 °C overnight. The pH of the washing water was 6.9. The dried precipitate was mixed with a stoichiometric amount of Li_2CO_3 (Alfa Aesar, 99%) and ground using an automatic grinder (Retsch RM-0). The precursors were heated in air at 900 °C for 3 h.

2.2. Materials Characterization. *2.2.1. X-ray Diffraction.* XRD patterns were collected with a Siemens D5000 diffractometer equipped with a Cu target X-ray tube and a diffracted beam monochromator. Samples for X-ray diffraction were prepared by adding powder to 2 mm deep × 25 mm × 20 mm "wells" in flat stainless steel plates. The powder was then packed and smoothed so that the sample surface was absolutely coplanar with the surface of the stainless steel plate. The stainless steel plates were registered on three alignment pins in the goniometer to ensure that the surface of the sample coincided with goniometer axis. The $Li[Ni_{1/3}Mn_{1/3}Co_{1/3-z}(MnMg)_{z/2}]O_2$ ($0 \le z \le 1/3$) samples were measured over a scattering angle range between 10 and 90° using 0.05° steps and a 30 s counting time. This long counting time was used so that small amounts of impurity phases, if present, could be detected.

2.2.2. Atomic Absorption Analysis. Atomic absorption spectroscopy, performed at the Minerals Engineering Center at Dalhousie University, was used to measure the (Mn+Mg):(Ni+Mn+Co+Mg) and Li: (Ni+Mn+Co+Mg) ratio in the heat-treated oxide. The procedures used have been shown to give a Li:Co ratio of 1.0:1.0 for stoichiometric $LiCoO_2$ samples obtained from battery materials suppliers. However, we do admit that this comparison does not guarantee that all Ni, Mn, Co, and Li atomic ratios will be perfectly accurate for the samples tested here. The estimated error in the Li:M ratio is about ±0.02.

2.2.3. SEM Imaging. A Hitachi S4700 field-emission scanning electron microscope (SEM) was used to image the materials.

2.2.4. Electrochemical Testing. Coin cells (23 mm diameter and 2.5 mm thick) were used for testing the electrochemical performance of the samples. Positive electrodes were prepared by mixing the active material, Super S Carbon Black, and PVDF in a weight ratio of 90:5:5. An appropriate amount of NMP was added to the mixture to form a slurry, which was then thoroughly mixed. The slurry was coated on Al foil and dried overnight in an oven. The electrochemical cells used a single lithium metal foil used as the counter electrode, Celgard 2320 microporous film as the separator and 1 M $LiPF_6$ in ethylene carbonate (EC) and diethyl carbonate (DEC) (1:2,v/v) (Novolyte Technologies) as the electrolyte. Cells were assembled in an argon-filled glovebox. The cells were removed from the glovebox and connected to a computer-controlled charging system (E-One/Moli Energy). The cells were initially charged and discharged at a $C/20$ rate in the range of 3.3 to 4.3 V or 3.3 to 4.6 V vs Li metal for two cycles. After the first two cycles, the charge−discharge rate was increased to $C/5$.

2.2.5. Thermal Stability Testing by Accelerating Rate Calorimetry. Preparation of Delithiated Positive Electrode Materials. The $Li[Ni_{1/3}Mn_{1/3}Co_{1/3-z}(MnMg)_{z/2}]O_2$ samples were delithiated electrochemically. Positive electrodes were prepared by mixing the active material, Super S Carbon Black, and PVDF in a weight ratio of 90:5:5. An appropriate amount of NMP was added to the mixture to form a slurry, which was then thoroughly mixed. The mixture was dried at 120 °C for 24 h. The dried mixture, containing positive electrode material, carbon black, and PVDF, was ground and was passed through a 300 μm opening stainless steel sieve. About 260 mg of the sieved powder was poured into a stainless steel pellet press and 1000−2000 psi was applied to make a 13 mm diameter × 1 mm thick electrode pellet. Pellet coin cells were made as described in ref 26. Figure 1 shows the structure of the pellet coin cells.

A recharge signature curve charge method was used to make delithiated $Li[Ni_{1/3}Mn_{1/3}Co_{1/3-z}(MnMg)_{z/2}]O_2$ samples. The pellet cells were charged to 4.3 V versus lithium using a current of 1.0 mA/g. After reaching 4.3 V, the cells were allowed to relax for 30 min, and then were charged to 4.3 V again at half of the first charge current. This process was repeated four times. After the charge was completed, the coin cells were opened in an

(22) Oh, S. H.; Lee, S. M.; Cho, W. I.; Cho, B. W. *Electrochim. Acta* **2006**, *51*, 3637.
(23) Bang, H. J.; Park, B. C.; Prakash, J.; Sun, Y. K. *J. Power Sources.* **2007**, *174*, 565.
(24) Jeong, K. H.; Ha, H. W.; Yun, N. J.; Hong, M. Z.; Kim, K. *Electrochim. Acta* **2005**, *50*, 5349.
(25) Luo, W.; Dahn, J. R. **2010**, in preparation.
(26) Richard, M. N.; Dahn, J. R. *J. Electrochem. Soc.* **1999**, *146*, 2068.

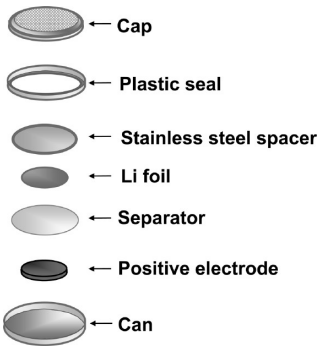

Figure 1. Exploded view of the structure of a coin cell containing a pellet electrode used for preparing charged samples for accelerating rate calorimetry.

argon-filled glovebox and disassembled. The wet pellet was ground lightly in a mortar and pestle and the resulting powder was poured into a centrifuge tube. The electrode powder was rinsed with dimethyl carbonate (DMC) four times and was separated by centrifuging for 3 min each time (centrifuge at 13 000 rpm, MSE Micro Centaur, Sanyo). The residual DMC was removed under vacuum in the antechamber of the glovebox at room temperature by pumping for about 2 h.

ARC Sample Preparation. The thermal stability of $Li[Ni_{1/3}Mn_{1/3}Co_{1/3-z}(MnMg)_{z/2}]O_2$ samples were tested using accelerating rate calorimetry (ARC).[27] ARC samples were made in 6.35 mm (0.250 in) outer diameter stainless steel (type 304) seamless tubing having a wall thickness of 0.15 mm (0.006 in.) (MicroGroup, Medway, MA). The stainless steel tubing was cut into 39 mm (1.54 in.) long pieces. The sample tubing was sonicated in acetone solution two times (for cleaning) and then dried in an oven at 100 °C. One end of the tubing was flattened and then welded shut inside an argon-filled glovebox by tungsen inert gas (TIG) welding using a Miller Maxstar 91 ARC welder, equipped with a Snap Start II high frequency ARC starter. After 94 mg of charged cathode material and 30 mg 1 M $LiPF_6$ EC: DEC electrolyte were added to the tubing, the other end of the tubing was clamped and welded closed while the tube was held in a copper heat sink block to prevent heating of the sample. All the welding steps were performed in an argon-filled glovebox. The welded ARC tubings were weighed before and after ARC experiments to ensure that no leaking had occurred. The ARC starting temperature was set to either 70 or 180 °C. Exothermic reactions were tracked under adiabatic conditions when the sample SHR exceeded 0.03 °C/min. Experiments were stopped at 350 °C or when the self-heating rate (SHR) was higher than 20 °C/min.

3. Results and Discussion

Figure 2 shows the XRD patterns of the $Li[Ni_{1/3}Mn_{1/3}Co_{1/3-z}(MnMg)_{z/2}]O_2$ ($0 \le z \le 1/3$) samples in the scattering angle range between 10 and 90°. In order to observe the characteristic peaks clearly, expanded views of the (101), (006), (012), (018), (110), and (113) Bragg peaks are given in Figure 3. In addition, an expanded view, on a sensitive vertical scale, is given of the region where impurities like Li_2CO_3 are known to appear. All of the peaks in Figures 2 and 3 can be indexed based on a hexagonal α-$NaFeO_2$ structure (space group: $R3\bar{M}$). A

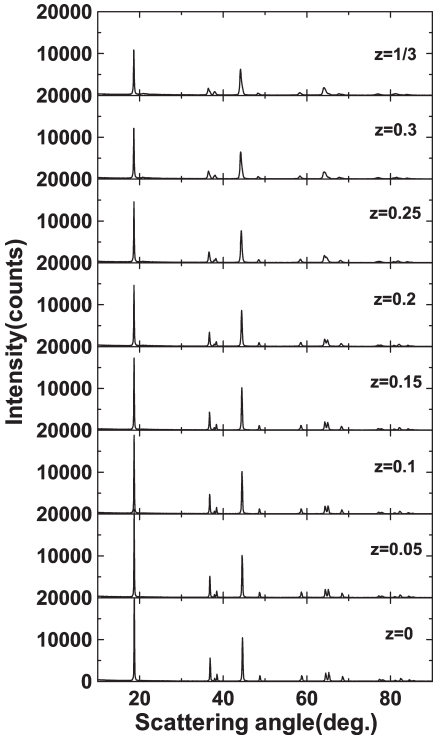

Figure 2. XRD patterns of $Li[Ni_{1/3}Mn_{1/3}Co_{1/3-z}[MnMg]_{z/2}]O_2$ ($0 \le z \le 1/3$) samples (10−90°).

broad weak XRD peak (indicated by the triangle) around 20.7° is presumably caused by the short-range ordering of Li, Ni, Co, Mn, and Mg in the transition-metal layers for $z \ge 0.2$. As z increases past $z = 0.25$, the 018 and 110 peaks appear to merge into a single peak. However, there may be small peaks near 65.0° and near 68.5° that may come from an impurity phase in the $z = 0.3$ and $z = 0.33$ samples. A careful examination of the middle column in Figure 3 also shows that the 006 and 012 peaks also appear to merge into a single peak as z increase past $z = 0.25$. There may also be a hint of a second phase in the $z = 0.3$ and $z = 0.33$ patterns as evidenced by the shoulder, near 36.8°, on the right side of the 101 peak. Therefore, it may be possible that the samples with $z = 0.3$ and $z = 0.33$ are not perfectly phase-pure. We believe that single phase $Li[Ni_{1/3}Mn_{1/3}Co_{1/3-z}(MnMg)_{z/2}]O_2$ samples can be prepared for $0 \le z \le 0.25$ and probably for $0 \le z \le 0.33$.

Figure 4 shows the lattice constants (a and c) as a function of z in $Li[Ni_{1/3}Mn_{1/3}Co_{1/3-z}(MnMg)_{z/2}]O_2$ ($0 \le z \le 1/3$) for the samples described by Figures 2 and 3. The lattice constants were determined by least-squares refinements to the measured positions of at least 10 Bragg peaks using in-house software, HEXOFF. The lattice constants, a and c, increase as z increases. The lattice constant, a, exhibits a linear variation versus composition. The lattice constant, c, varies smoothly with z for the samples for $0 \le z \le 1/3$. Both lattice constants increase with z since the average ionic radii of Mn^{4+} and Mg^{2+} are larger than that of Co^{3+} ($r_{Mg}{}^{2+} = 0.72$ Å, $r_{Mn}{}^{4+} = 0.53$ Å, $r_{Co}{}^{3+} = 0.545$ Å).[28] The results in Figures 2−4 suggest that Mn + Mg

(27) MacNeil, D. D. Ph. D. Thesis, Dalhousie University, 2001.

(28) Shannon, R. D. *Acta Crystallogr., Sect. A* **1976**, *32*, 751–767.

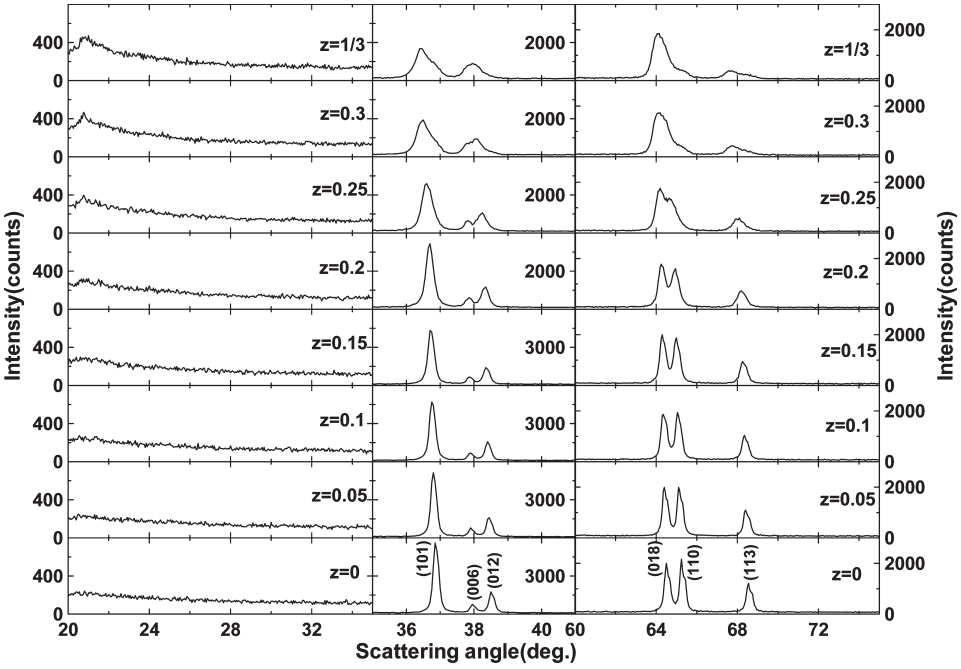

Figure 3. XRD patterns of $Li[Ni_{1/3}Mn_{1/3}Co_{1/3-z}[MnMg]_{z/2}]O_2$ ($0 \leq z \leq 1/3$) (20−35°, 35−41°, and 6−75°). Notice the change in vertical scale from panel to panel.

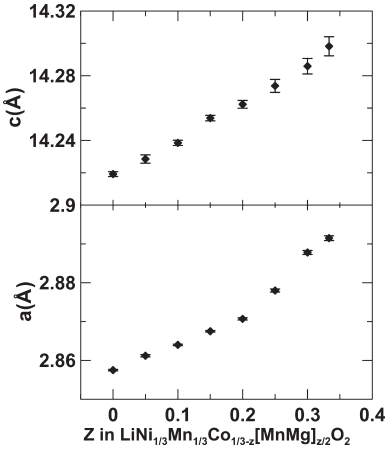

Figure 4. Lattice constants of $Li[Ni_{1/3}Mn_{1/3}Co_{1/3-z}[MnMg]_{z/2}]O_2$ ($0 \leq z \leq 1/3$) versus z.

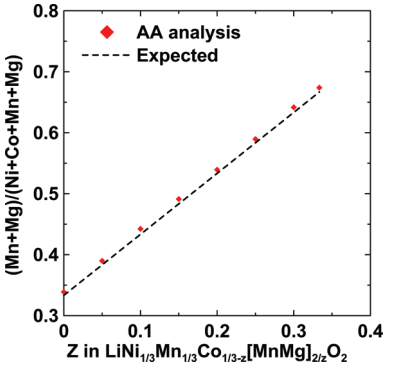

Figure 5. (Mn+Mg):(Ni+Co+Mn+Mg) ratio measured by AA analysis plotted versus that expected from synthesis for all the $LiNi_{1/3}Mn_{1/3}Co_{1/3-z}[MnMg]_{z/2}O_2$ ($0 \leq z \leq 1/3$) samples prepared in this work.

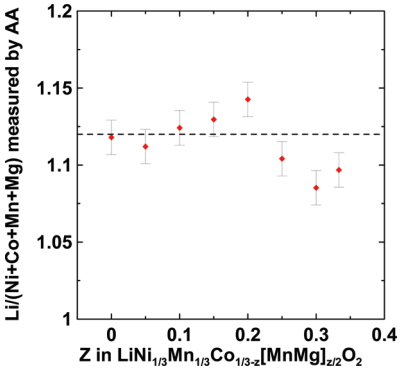

Figure 6. Li:(Ni+Co+Mn+Mg) ratio measured by AA analysis plotted versus that expected from synthesis for all $Li[Ni_{1/3}Mn_{1/3}Co_{1/3-z}[MnMg]_{z/2}]O_2$ ($0 \leq z \leq 1/3$) samples prepared in this work.

can substitute for Co in $Li[Ni_{1/3}Mn_{1/3}Co_{1/3-z}(MnMg)_{z/2}]O_2$ for $0 \leq z \leq 1/3$ successfully.

Figure 5 shows the variation of the measured (Mn+Mg) content in the samples as measured by AA analysis compared to the expected content based on the molar ratios used during synthesis. The agreement is excellent, showing that the Mn and Mg are incorporated within the final oxide samples.

Figure 6 shows the variation of the Li content in the samples as measured AA analysis compared to the expected content based on the molar ratios used during synthesis. Figure 6 shows that Li content (the molar ratio of Li versus M (M = Ni+Mn+Co+Mg) ranged between about 1.09−1.14. This lithium excess occurred because it was impossible to recover all the coprecipitate during the washing and centrifuging process. The amount of lithium added to the coprecipitate was based on an expected full recovery. It appears that typically, only about 95% of the hydroxide was recovered. The outcome of this result is that all of the samples are about 5% rich in lithium, as calculated by x in $Li[Li_xM_{1-x}]O_2$.

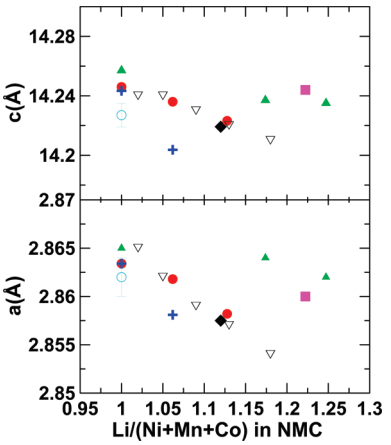

Figure 7. Lattice constants a and c versus the molar ratio Li:(Ni+Co+Mn+Mg). The $z = 0$ sample in this work that contains excess lithium is indicated by ♦. The results of this work are compared to the results from ●, ref 29; ▲, ref 30; +, ref 31; ■, ref 32; ○, ref 33; and ▽, ref 34.

According to the AAS results, the nominal $Li[Ni_{1/3}Mn_{1/3}Co_{1/3}]O_2$ sample ($z = 0$) contains excess Li and has Li/(Ni+Mn+Co) = 1.12. Figure 7 shows the lattice constants of $Li_{1+x}[Ni_{1/3}Mn_{1/3}Co_{1/3}]_{1-x}O_2$ samples measured in literature reports.[29−34] Where data extends beyond Li/(Ni+Mn+Co) = 1, a continuous decrease in the lattice parameters is observed as the value of Li/(Ni+Mn+Co) increases. The lattice constant obtained for our $z = 0$ sample, with Li/(Ni + Mn + Co) = 1.12 matches the behavior shown in Figure 7 very well. This gives further confidence in the AAS results. The lattice constants decrease with Li/(Ni+Mn+Co) because the ionic radius of Ni^{3+} is smaller than that of Ni^{2+}($r_{Ni}^{2+} = 0.69$ Å, $r_{Ni}^{3+} = 0.56$ Å).[28]

To further understand the influence of the Mn and Mg cosubstitutions on the structure of these materials, we carried out Rietveld refinements for $z = 0$ to 0.2 samples. The crystal structure was refined by the Rietveld method using the software "Rietica for Windows", version 1.7.7. We assumed Li on 3a sites, a small amount of Li (excess Li), Ni, Co, Mn, and Mg on 3b sites, and oxygen on 6c sites. The AA analysis results suggest these materials have a Li excess. Our previous studies show that Co, Mn, and Mg can not enter the Li layers in the $Li[Ni_{1/3}Mn_{1/3}Co_{1/3-z}Mg_z]O_2$ and $Li[Co_{1-z}(MnMg)_{z/2}]O_2$ systems.[17,35] The refinements allow for a small amount of transition metal atoms (Ni) on the 3b sites (in the transition metal layer) to exchange with Li on the 3a sites (in the Li layer). Thus, the nominal formula of $Li[Ni_{1/3}Mn_{1/3}Co_{1/3-z}(MnMg)_{z/2}]O_2$, for example, is assumed to be as follows: $[Li_{1-\delta}Ni_\delta]_{3a}[Li_{x+\delta}(Mn_{1/3}Co_{1/3-z}Mn_{z/2}Mg_{z/2})_{1-x}Ni_{(1-x)/3-\delta}]_{3b}O_2$. In the formula $[Li_{1-\delta}Ni_\delta]_{3a}[Li_{x+\delta}(Mn_{1/3}Co_{1/3-z}Mn_{z/2}Mg_{z/2})_{1-x}Ni_{(1-x)/3-\delta}]_{3b}O_2$, x (fixed) is the overlithiation ratio as determined by AAS analysis and δ (which was refined) is the nickel occupancy in the lithium site. The presence of δ Ni atoms in the 3a site implies δ Li atoms in the 3b site (i.e., an exchange between Li and Ni). As a result, the total Li occupation in the 3b site is equal to $x+\delta$. For the refinement of the XRD data, the 3a and 3b sites were constrained to be full. The total lithium concentration and the nickel concentration were constrained to be $1+x$ and $(1-x)/3$, respectively. The total manganese, cobalt, and magnesium occupations were fixed to be $(1/3+z/2)$-$(1-x)$, $(1/3-z)(1-x)$ and $(1-x)z/2$, respectively. Pseudo-Voight peak shapes and no peak asymmetry were used. According the to AA analysis results and the structural model above, the starting structural formulas are shown in Table 2. The final results of the refinements are also given in Table 2.

Figure 8 shows the typical agreement between the observed and calculated XRD patterns using the $Li[Ni_{1/3}Mn_{1/3}Co_{1/3}]O_2$, $Li[Ni_{1/3}Mn_{1/3}Co_{0.23}(MnMg)_{0.05}]O_2$ and $Li[Ni_{1/3}Mn_{1/3}Co_{0.13}(MnMg)_{0.1}]O_2$ samples as examples. This suggests that the structural model is correct.

Figure 9 shows the variation of transition metal content in the Li layers for $Li[Ni_{1/3}Mn_{1/3}Co_{1/3-z}(MnMg)_{z/2}]O_2$ ($0 \le z \le 0.2$). For the unsubstituted $Li[Ni_{1/3}Mn_{1/3}Co_{1/3}]O_2$ (NMC) sample, the transition metal content in the Li layer is 0.93%. When Mn+Mg substitutes for Co in NMC, there is a strong increase in the amount of transition metal in the Li layer. These results are consistent with previous work.[17]

Figure 10 shows scanning electron micrographs of three of the samples studied here. Images A1 and A2 in Figure 10 show the morphology of the $Li[Ni_{1/3}Mn_{1/3}Co_{1/3}]O_2$ sample. Images B1 and B2 in Figure 10 show the morphology of the $Li[Ni_{1/3}Mn_{1/3}Co_{0.23}[MnMg]_{0.05}]O_2$ sample. Images C1 and C2 in Figure 10 show the morphology of the $LiNi_{1/3}Mn_{1/3}Co_{0.13}[MnMg]_{0.1}O_2$ sample. The samples in Figure 10A−C show crystallites with flat facets, having primary particle sizes around 300 nm. The level of substitution had no discernible impact on particle morphologies and particle size.

Figure 11 compares the first charge and discharge curves of $Li[Ni_{1/3}Mn_{1/3}Co_{1/3-z}(MnMg)_{z/2}]O_2$ ($0 \le z \le 1/3$) for different composition in the range of $0 \le z \le 1/3$ using a specific current of $C/20$. The red dashed line and the black solid line show results for the voltage ranges 3.3−4.3 V and 3.3−4.6 V, respectively. The coin cell results in Figure 11 for the first charge to 4.3 V should be exactly the same for the cell charged to 4.3 V and the cell charged to 4.6 V (for samples with the same z). All pairs of cells having the same value of z agree well during the first charge, except for the pair of cells with $z = 0.05$. This suggests that some error in determining the electrode mass or in cell assembly occurred for this pair of cells. Thus, the results for the cells with $z = 0.05$ should be given less weight than those of the other compositions.

All the samples described in Figure 11 show smooth charge−discharge curves. The $z = 0$ sample has the smallest charge−discharge polarization and the smallest irreversible capacity of all the samples. The samples show

(29) Gozu, M.; Swierczek., K.; Molenda., J. *J. Power Sources* **2009**, *194*, 38.
(30) Kim, J. M.; Kumagai, N.; Chung, H. T. *Electrochem. Solid-State Lett*. **2006**, *9*, A494.
(31) Choi., J.; Manthiram., A. *Electrochem. Solid-State Lett*. **2004**, *7*, A365.
(32) Chen., Z.; Sun., Y. K.; Amine., K. *J. Electrochem. Soc*. **2006**, *153*, A1818.
(33) Yabuuchi, N.; Ohzuku, T. *J. Power Sources*. **2003**, *119*, 171.
(34) Todorov., Y. M.; Numata., K. *Electrochimica acta*. **2004**, *50*, 495.
(35) Luo, W.; Dahn, J. R. J. Electrochem. Soc. **2010**, submitted.

Table 1. Lattice Constants and Specific Surface Areas of $Li[Ni_{1/3}Mn_{1/3}Co_{1/3-z}(MnMg)_{z/2}]O_2$ Samples

nominal chemical composition	Z	a (Å)	c (Å)	specific surface area (m^2/g)
$LiNi_{1/3}Mn_{1/3}Co_{1/3-z}(MnMg)_{z/2}O_2$	0	2.8575(2)	14.2192(15)	2.47
	0.05	2.8612(3)	14.2285(26)	
	0.1	2.8640(2)	14.2385(16)	3.94
	0.15	2.8675(2)	14.2538(17)	
	0.2	2.8707(3)	14.2623(24)	2.93
	0.25	2.878(4)	14.2737(40)	
	0.3	2.8878(5)	14.2859(48)	
	1/3	2.8915(6)	14.2982(59)	

Table 2. Rietveld Refinements of $Li[Ni_{1/3}Mn_{1/3}Co_{1/3-z}(MnMg)_{z/2}]O_2$ with $z = 0$, 0.05, 0.1, 0.15, and 0.2[a]

	$Z = 0$		$Z = 0.05$		$Z = 0.1$		$Z = 0.15$		$Z = 0.2$	
parameter	initial	final	initial	final	initial	final	initial	final	initial	final
Li 3a	*1*	*0.991(1)*	*1*	*0.981(1)*	*1*	*0.974(1)*	*1*	*0.965(1)*	*1*	*0.954(1)*
Ni 3b	*0.313*	*0.304(1)*	*0.317*	*0.298(1)*	*0.313*	*0.287(1)*	*0.313*	*0.278(1)*	*0.312*	*0.266(1)*
Mn 3b	0.313	0.313	0.340	0.340	0.360	0.360	0.384	0.384	0.405	0.405
Co 3b	0.314	0.314	0.269	0.269	0.220	0.220	0.172	0.172	0.125	0.125
Mg 3b	0	0	0.024	0.024	0.047	0.047	0.071	0.071	0.093	0.093
Li 3b	*0.06*	*0.069(1)*	*0.05*	*0.069(1)*	*0.06*	*0.086(1)*	*0.06*	*0.095(1)*	*0.065*	*0.111(1)*
Ni 3a	*0*	*0.009(1)*	*0*	*0.019(1)*	*0*	*0.026(1)*	*0*	*0.035(1)*	*0*	*0.046(1)*
R_B	1.67		1.38		1.39		1.65		2.48	
R_{wp}	8.28		8.10		8.32		8.99		9.78	
R_p	6.0		5.656		6.02		6.33		7.19	
χ^2	1.89		1.80		1.93		2.28		2.62	

[a] The site occupations before and after refinement are given. The Bragg agreement factor, R_B, the weighted-profile R value, R_{wp}, and the goodness-of-fit, χ^2, are also listed. Parameters that were refined are in italics. Refinement constraints were included so that the number of cations and oxygen atoms in the unit cell were equal and so that number of Li and Ni atoms before and after refinement were equal.

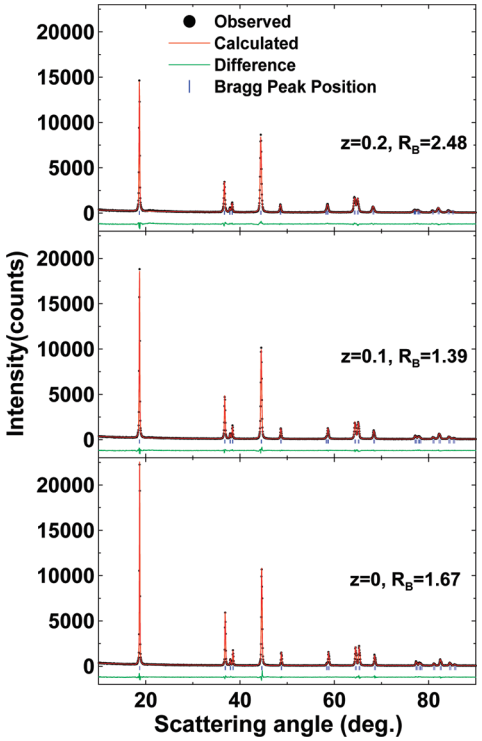

Figure 8. Rietveld refinement results for $Li[Ni_{1/3}Mn_{1/3}Co_{1/3-z}(MnMg)_{z/2}]O_2$ with $z = 0$, 0.1, and 0.2 samples.

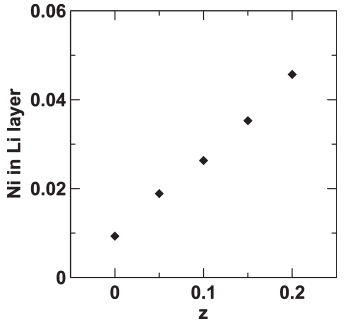

Figure 9. Transition metal content in the Li layer of $Li[Ni_{1/3}Mn_{1/3}Co_{1/3-z}(MnMg)_{z/2}]O_2$ ($0 \le z \le 0.2$) plotted versus z, obtained by Rietveld refinements.

good reversibility when charged to 4.3 V. The samples show larger irreversible capacity with increasing z in $Li[Ni_{1/3}Mn_{1/3}Co_{1/3-z}(MnMg)_{z/2}]O_2$. When charged to 4.6 V, a plateau develops near 4.5 V during the first charge as z increases. This plateau does not appear to be reversible and may be associated with the simultaneous removal of Li and oxygen from the material. Further research is required to understand the origin of this plateau.

Figure 12 shows the capacity versus cycle number for $Li/Li[Ni_{1/3}Mn_{1/3}Co_{1/3-z}(MnMg)_{z/2}]O_2$ ($0 \le z \le 0.25$) cells in the voltage ranges 3.3−4.3 V (left panels) and 3.3−4.6 V (right panels). For all the samples studied, the discharge capacity drops during the first several cycles, but remains relatively stable in the following cycles. There seems to be no advantage in cycle life caused by simultaneous Mn−Mg substitution.

Figure 13 shows the differential capacity versus potential of the same samples described by Figure 11 plotted versus potential. The red dashed line shows the differential capacity vs potential for cells charged to 4.3 V. For all samples, apart from small differences between the first charge cycle and second cycle thought to be caused by the impedance of the uncycled Li electrode in the freshly assembled cells, the differential capacity is perfectly

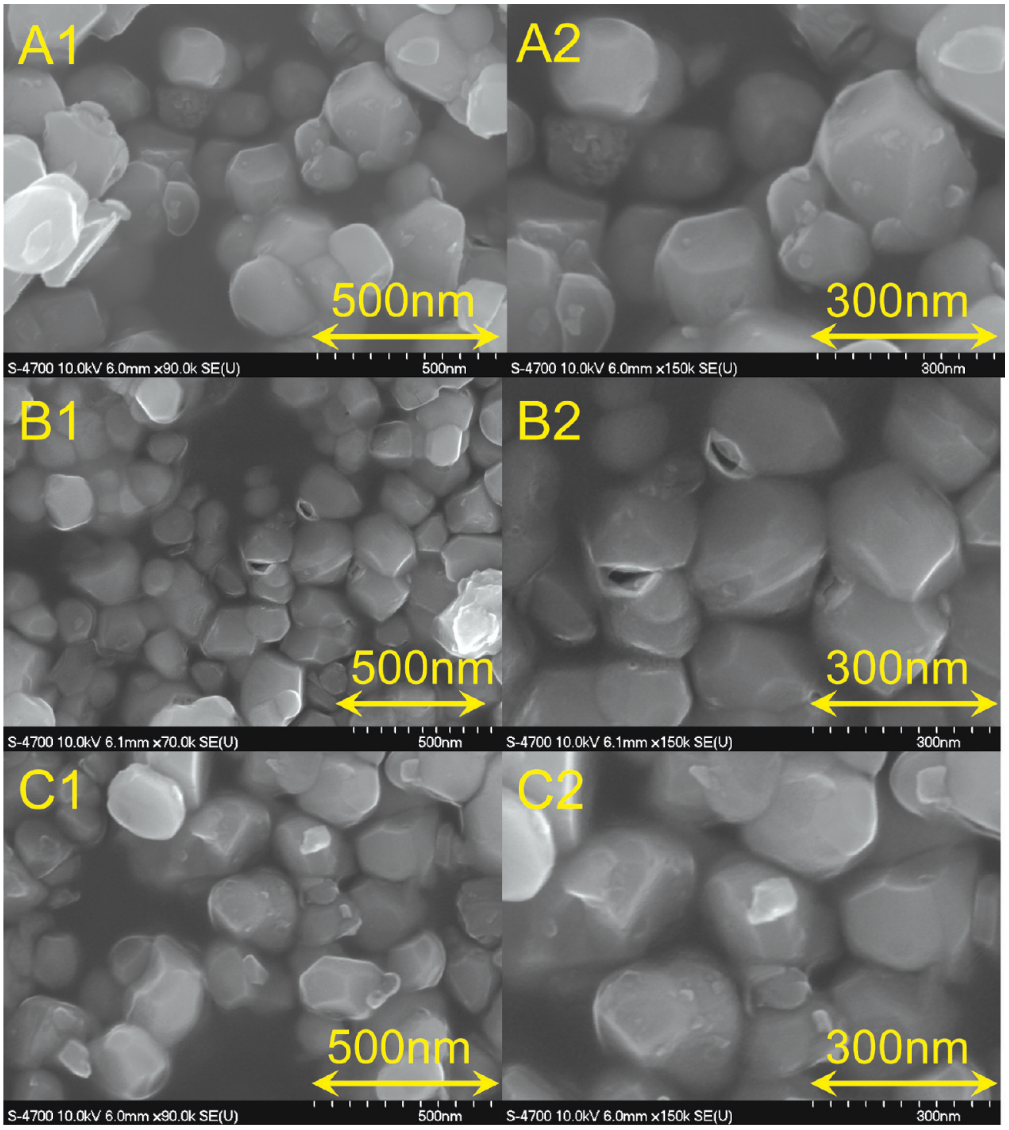

Figure 10. SEM images of (A) $Li[Ni_{1/3}Mn_{1/3}Co_{1/3}]O_2$, (B) $Li[Ni_{1/3}Mn_{1/3}Co_{0.23}[MnMg]_{0.05}]O_2$, (C) $Li[Ni_{1/3}Mn_{1/3}Co_{0.13}[MnMg]_{0.1}]O_2$.

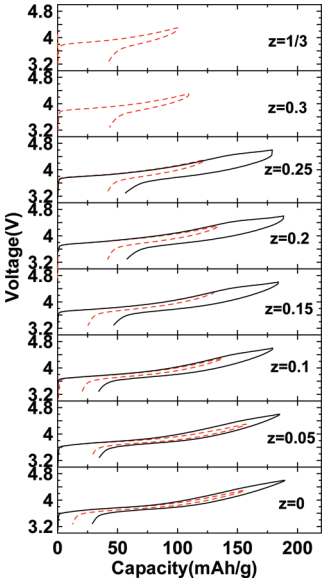

Figure 11. Potential (V) vs specific capacity (mA h/g) of $Li/Li[Ni_{1/3}Mn_{1/3}Co_{1/3-z}[MnMg]_{z/2}]O_2$ ($0 \le z \le 1/3$) cells cycled between 3.3 to 4.3 V (red dashed line) and 3.3 to 4.6 V (black solid line) at a rate of C/20.

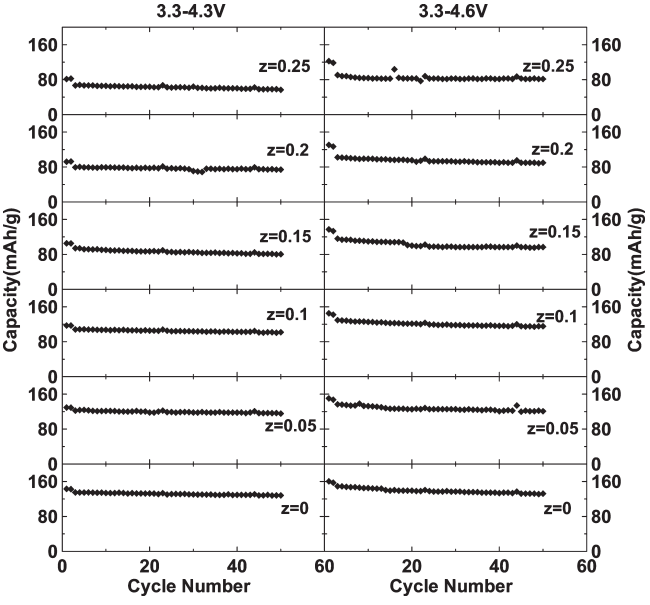

Figure 12. Specific discharge capacity vs cycle number curves of $Li/Li[Ni_{1/3}Mn_{1/3}Co_{1/3-z}[MnMg]_{z/2}]O_2$ ($0 \le z \le 0.25$) cells.

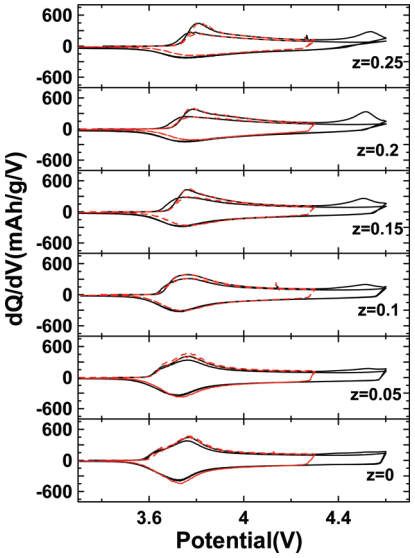

Figure 13. Differential capacity (dQ/dV) vs potential (V) of Li/Li[$Ni_{1/3}Mn_{1/3}Co_{1/3-z}[MnMg]_{z/2}]O_2$ ($0 \le z \le 0.25$) cells cycled between 3.3−4.3 V (the red dashed line) and 3.3−4.6 V (the black solid line) at a rate of $C/20$. The first two charge−discharge cycles are shown.

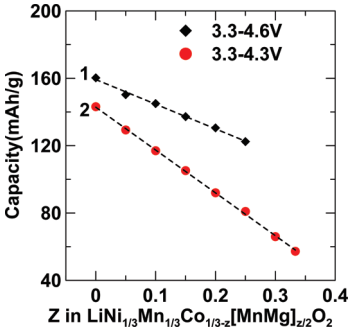

Figure 14. First discharge capacities as a function of z in of Li[$Ni_{1/3}Mn_{1/3}Co_{1/3-z}[MnMg]_{z/2}]O_2$ ($0 \le z \le 1/3$) samples. Results for cells charged to 4.3 and 4.6 V are shown as indicated.

repeatable for numerous cycles, suggesting a stable intercalation process for all these materials when charged to 4.3 V. The black solid line shows the differential capacity vs potential of the first charge to 4.6 V is different than the next cycle. The appearance of a broad peak in dQ/dV when z increases, may be associated with with oxygen loss from the oxide and a simultaneous Li^+ extraction.[36] P. Novak et al. confirmed oxygen evolution for overlithiated NMC compounds and no oxygen evolution for the stoichiometic NMC compounds.[37] Our previous research indicated oxygen loss when overlithiated Li[Co_{1-z}-(MnMg)]$_{z/2}O_2$ electrodes were charged to 4.5 V using in situ XRD.[35]

Figure 14 shows the variation of the first discharge capacity (3.3−4.3 V or 3.3−4.6 V, C/20) versus z in Li[$Ni_{1/3}Mn_{1/3}Co_{1/3-z}(MnMg)_{z/2}]O_2$ ($0 \le z \le 1/3$) samples. The slope of the dashed line "1" in the Figure is −150 (mAh/g)/(z = 1). The slope of the dashed line "2" in the Figure is −250 (mA h/g)/(z = 1). In reference[17] the

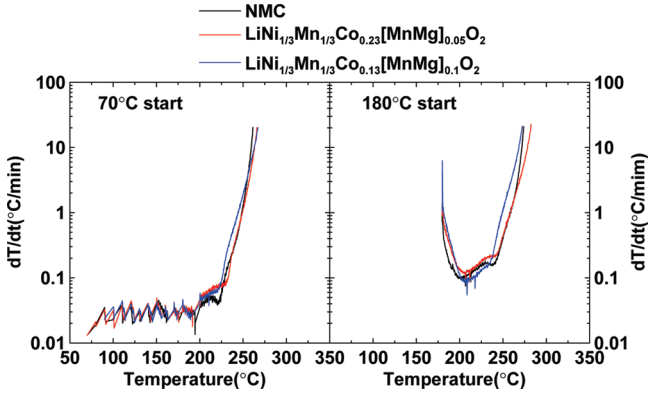

Figure 15. The self-heating rate versus temperature for the Li[$Ni_{1/3}Mn_{1/3}Co_{1/3-z}[MnMg]_{z/2}]O_2$ (z = 0, 0.1, 0.2) samples charged to 4.3 V reacting with 30 mg of 1 M $LiPF_6$ EC:DEC electrolyte with starting temperatures of 70 and 180 °C.

specific capacity of Mg substituted Li[$Ni_{1/3}Mn_{1/3}Co_{1/3}]O_2$ was plotted versus the Mg content. It was shown that the capacity decreased with a slope of about −390 (mA h/g)/(z = 1), which is more than that found here for Mn and Mg cosubstitution. Because the average transition metal oxidation state in $LiMO_2$ is M^{3+}, substituting Mg as Mg^{2+} for Co adds one inactive cation and also causes a corresponding increase in the average oxidation state of the transition metal cations. Substituting equal amounts of Mg as Mg^{2+} and Mn as Mn^{4+} for Co^{3+}, the average oxidation state of the transition metals is unchanged. Compared with pure Mg substitution, Mn and Mg cosubstitution only adds inactive cations and does not cause a corresponding increase in the average oxidation state of the transition metal cations. This helps explain why the rate of capacity reduction with substiuent concentration (Mn+Mg) is the smallest we have seen so far.

Figure 15 shows the self-heating rate versus temperature for the Li[$Ni_{1/3}Mn_{1/3}Co_{1/3-z}[MnMg]_{z/2}]O_2$ (z = 0, 0.1, 0.2) samples charged to 4.3 V reacting with 30 mg of 1 M $LiPF_6$ EC:DEC electrolyte with starting temperatures of 70 or 180 °C. A 180 °C start temperature was included in an attempt to study the thermal stability of Li[$Ni_{1/3}Mn_{1/3}Co_{1/3-z}[MnMg]_{z/2}]O_2$ under forced heating conditions. Figure 15 shows that when no Mn and Mg are added, the material reacts dramatically with 1 M $LiPF_6$ EC:DEC [1:2 v/v] when the temperature is higher than 230 °C, leading to an extremely rapid temperature rise beyond the maximum heating rate of the ARC. Figure 15 shows that the thermal stability is not affected as z is changed for experiments started at either 70 or 180 °C. According to the literature, the thermal stability of charged positive electrode materials normally decreases with increasing specific surface area.[38] Therefore, the surface area is a very important factor for studies of thermal stability. Table 1 shows that the surface area of the samples described by Figure 15 is 3.2 ± 0.7 m^2/g. Therefore, we do not believe that the minor differences between the thermal stability of the samples could

(36) Lu, Z.; MacNeil, D. D.; Dahn, J. R. *Electrochem. Solid-State Letters* **2001**, *4*, A191.
(37) Mantia, F. L.; Rosciano, F.; Tran, N; Novak, P. *J. Electrochem. Soc.* **2009**, *156*, A823.
(38) MacNeil, D. D.; Larcher, D.; Dahn, J. R. *J. Electrochem. Soc.* **1999**, *146*, 3596.

becaused by differences in surface area. The results in Figure 15 indicate that cosubstituting Mn and Mg for Co in NMC-type materials is unlikely to lead to increases in the thermal stability of charged electrode materials in electrolyte.

4. Conclusions

A full series of $Li[Ni_{1/3}Mn_{1/3}Co_{1/3-z}(MnMg)_{z/2}]O_2$ ($0 \leq z \leq 1/3$) samples were prepared from hydroxide precursors. The hydroxide precursors were heated with Li_2CO_3 at 900 °C for 3 h to prepare the oxides. $Li[Ni_{1/3}Mn_{1/3}Co_{1/3-z}(MnMg)_{z/2}]O_2$ samples were pure single phases for $0 \leq z \leq 1/3$. The lattice constants a and c increase as z increases, which shows that Mn+Mg can substitute successfully for Co in $Li[Ni_{1/3}Mn_{1/3}Co_{1/3-z}(MnMg)_{z/2}]O_2$ over a wide range of $0 \leq z \leq 1/3$.

The AA analysis experiments show that these materials contain an excess of Li. The outcome of this result is that all of the samples are about 5% rich in lithium as measured by x in $Li[Li_xM_{1-x}]O_2$. Rietveld refinements of XRD data show that when Mn and Mg substitute for Co in NMC there is an increase in the amount of transition metal in the Li layer.

Electrochemical studies of the $Li[Ni_{1/3}Mn_{1/3}Co_{1/3-z}(MnMg)_{z/2}]O_2$ ($0 \leq z \leq 0.3$) samples were used to measure the rate of capacity reduction with Mn and Mg content, found to be about -250 (mA h/g)/($z = 1$) when charged to 4.3 V and -150 (mA h/g)/($z = 1$) when charged to 4.6 V.

The reactivity of charged $Li[Ni_{1/3}Mn_{1/3}Co_{1/3-z}(MnMg)_{z/2}]O_2$ samples with electrolyte was measured using accelerating rate calorimetry. There is no discernible change in thermal stability as z increases. Therefore, based on all the results in this report, we conclude that simultaneous Mn and Mg substitution for Co in NMC-type positive electrode materials is not beneficial.

Acknowledgment. The authors thank NSERC and 3M Canada for funding this work under the auspices of the Industrial Research Chair program. W.L. thanks the China Scholarship Council for scholarship support.